Quaternary Science Reviews 125 (2015) 78–90

Contents lists available at ScienceDirect

Quaternary Science Reviews

journal homepage: www.elsevier.com/locate/quascirev

Pervasive multidecadal variations in productivity within the Peruvian Upwelling System over the last millennium

S. Fleury [a, *], P. Martinez [a], X. Crosta [a], K. Charlier [a], I. Billy [a], V. Hanquiez a, T. Blanz [b], R.R. Schneider [b]

[a] Université de Bordeaux, CNRS, UMR 5805 EPOC, Allée Geoffroy Saint-Hilaire, 33615 Pessac, France
[b] Institut für Geowissenschaften, Christian-Albrechts Universität-zu-Kiel, Ludewig-Meyn-Strasse 10, 24118 Kiel, Germany

ARTICLE INFO

Article history:
Received 15 December 2014
Received in revised form
17 July 2015
Accepted 6 August 2015
Available online xxx

Keywords:
Laminations
Decadal variability
El Niño–Southern Oscillation
Intertropical Convergence Zone
Walker circulation
Atlantic Meridional Overturning Circulation
North Atlantic Oscillation

ABSTRACT

There is no agreement on the pluri-decadal expression of El Niño–Southern Oscillation (ENSO) in the Pacific over the last millennium. Marine records from the Peruvian margin indicate humid conditions (El Niño-like mean conditions) over the Little Ice Age, while precipitation records from the eastern equatorial Pacific infer arid conditions (La Niña-like mean conditions) for the same period. We here studied diatom assemblages, nitrogen isotopes, and major and minor elements at the lamination level in three laminated trigger cores located between 11°S and 15°S on the Peruvian shelf within the oxygen minimum zone (OMZ) to reconstruct precipitation and ocean productivity at the multiannual to multidecadal timescales over the last millennium. We respected the sediment structure, thus providing the first records of the mean climatic conditions at the origin of the lamination deposition, which ones represent several years. Light laminations were deposited under productive and dry conditions, indicative of La Niña-like mean conditions in the system, while dark laminations were deposited under non-productive and humid conditions, representative of El Niño-like mean conditions. La Niña-like mean conditions were predominant during the Medieval Warm Period (MWP; 1000–600 years BP) and Current Warm Period (CWP; 150 years BP to present), while El Niño-like mean conditions prevailed over the Little Ice Age (LIA; 600–150 years BP). We provide evidence for persistent multidecadal variations in productivity over the last millennium, which were disconnected from the mean climate state. Multidecadal variability has been stronger over the last 450 years concomitantly to increased variability in the NAO index. Two intervals of strong multidecadal variability were also observed over the MWP, congruent to decreased solar irradiance and increased volcanic activity.

1. Introduction

The last millennium has been divided into several climatic periods, based on warmer global conditions over the Medieval Warm Period (MWP), colder temperatures over the Little Ice Age (LIA) and rising temperatures since the beginning of the Current Warm Period (CWP) (e.g. Jones et al., 1998; Mann et al., 1999). Most studies indicate a CWP beginning around AD 1800–1850 but there is no agreement on the exact temporal extent of the MWP and the LIA. Glacier extent and temperature reconstructions from historical sources place the limit between the MWP and the LIA around AD 1250–1270 (Grove, 1988; Lamb, 1985) while Greenland ice cores rather date the onset of the LIA around AD 1350 (Stuiver et al., 1995). Finally, North American records place the MWP between AD 1100 and AD 1375 and the LIA between AD 1450 and AD 1850 (Davis, 1994; Graumlich, 1993). The onset of the LIA has been extensively studied and is generally attributed to reduced solar activity (e.g. Mann et al., 2005; Swingedouw et al., 2011), although alternative hypotheses also suggest changes in the inflow of North Atlantic water into the Nordic Seas (Jungclaus et al., 2005). At lower latitudes, solar-driven temperature variations are thought to have induced changes in wind patterns and rainfall intensity. The northeastern trade winds would have been stronger during the LIA, leading to the southward migration of the Intertropical Convergence Zone (ITCZ) (Sachs et al., 2009) and aridity in the northern tropics, marked by droughts in southeast Asia (Zhang et al., 2008), east Africa (Wolff et al., 2011) and the Yucatán Peninsula (Hodell

* Corresponding author.
E-mail addresses: sophie.fleury@u-bordeaux.fr, fleurysoph@hotmail.com (S. Fleury).

http://dx.doi.org/10.1016/j.quascirev.2015.08.006
0277-3791/

et al., 2005), as well as higher levels of precipitation in the southern tropics (Reuter et al., 2009).

These long-term hydrological changes have also been expressed in variations in El Niño–Southern Oscillation (ENSO). Existing records of ENSO provide contradictory information, however, both at the global and regional levels. Indeed, marine records from the Pacific Ocean indicate an LIA that was dominated either by arid conditions (La Niña-like mean state, Yan et al., 2011) or by humid conditions (El Niño-like mean state, Rein et al., 2004), while precipitation records from Ecuador evidence more frequent and stronger El Niño events over the MWP (Moy et al., 2002), despite decreased humidity in South America (Reuter et al., 2009). A possible explanation for the observed discrepancies could be that some records consider only El Niño events (Moy et al., 2002; Conroy et al., 2008) while other records also trace La Niña events (Cobb et al., 2003) and that the central Pacific is influenced both by the canonical El Niño (EP) and the El Niño Modoki (CP) (Ashok et al., 2007; Weng et al., 2007) while the eastern Pacific only records EP El Niño events (Dewitte et al., 2012). There, EP El Niño events (Kao and Yu, 2009) coincide with reduced upwelling intensity and decreased productivity off the coast of Peru (Pennington et al., 2006), as well as subsequent rises in Sea Surface Temperatures (SSTs) (Philander, 1990). The reduction in the upwelling of oxygen-depleted waters during EP El Niño events leads to an increase in the oxygen content of subsurface waters (Gutiérrez et al., 2008).

Published marine records from the Peru–Chile margin infer an MWP and a CWP dominated by La Niña-like mean conditions and an LIA dominated by El Niño-like mean conditions (e.g. Diaz-Ochoa et al., 2009; Salvatteci et al., 2014). These studies were based on discrete sampling, thus disregarding the sedimentary structures of the cores. Sediment from the oxygen minimum zones (OMZs) is finely laminated (Brodie and Kemp, 1994), enabling high-resolution records of variations in detrital and biogenic fluxes in relation to precipitation over the continent and upwelling intensity, respectively. We here study three trigger cores from the Peruvian OMZ at the lamination level in order to refine decadal to centennial variations in hydrology and productivity over the past millennium and propose possible forcing mechanisms.

2. Present-day characteristics of the study area

We here focus on the southern part (11–15°S) of the Peru–Ecuador margin, which extends from 1°N to 18°S along the west coast of South America (Fig. 1). In this region, trade winds blow northwestward and drive surface waters northward. This mechanism generates the Peru–Chile Coastal Current along the coast and the Peru–Chile Current further offshore (Fiedler and Talley, 2006). The Equatorial Undercurrent flows eastward under the surface waters; when it approaches South America, it is deflected southward, constituting the Peru–Chile Undercurrent. Similarly, the Southern Subsurface Countercurrent becomes the Peru–Chile Countercurrent when it starts flowing southward. The Peru–Chile Undercurrent sources the waters that are upwelled along the coast (Wyrtki, 1981; Toggweiler et al., 1991), which are characterized by low oxygen and high nutrient content. Oxygenation decreases when the currents circulate southward, which results in suboxic to anoxic subsurface waters south of 10°S (Fig. 1).

While subsurface oxygen concentrations decrease southward, contents in surface nutrients, in particular nitrates, increase northward. Productivity is more intense within the main upwelling region however (from 5 to 15°S and from the coast to 60 km offshore), where the nutrient-rich Peru–Chile Undercurrent is upwelled. The quantities of nutrients introduced into the Peruvian Upwelling System by the Peru–Chile Undercurrent are sufficient to sustain the highest production of chlorophyll-a and biomass in the world (Chavez and Barber, 1987; Chavez and Messié, 2009). The phytoplankton community is dominated by diatoms, especially the neritic bloom-forming *Chaetoceros* spp. (Cowles et al., 1977; Avaria and Muñoz, 1987).

Productivity varies throughout the year in response to seasonal variations in upwelling intensity combined with water mixing. The upwelling reaches its peak in austral winter (June, July, and August) (Messié et al., 2009), however biological production remains stable due to lower light availability caused by deeper mixing (Pennington et al., 2006). Concentrations in chlorophyll-a thus only reach their maximum in austral spring (Chavez et al., 1996; Echevin et al., 2008). However, these seasonal variations are low and high productivity levels are sustained throughout the year (Chavez, 1995), mainly because of the persistence of upwelling-favorable winds all year long (Strub et al., 1998). Interannual variations in phytoplankton productivity also occur, particularly under the influence of ENSO (Philander, 1990), which generates stronger variations than the ones observed at the seasonal timescale (Barber and Chavez, 1986). EP El Niño events lead to the persistence of warm surface waters offshore of Peru, despite the presence of winds favorable to upwelling (Strub et al., 1998). Upwelling still occurs but is restricted to a narrower area of the coast (Barber et al., 1996). The nutricline and thermocline are anomalously deep during EP El Niño events, causing the upwelling of warm, nutrient-poor waters. EP El Niño events lead to dramatic reductions in biological production and biomass as well as to changes in specific composition (Cowles et al., 1977) compared to normal conditions. In contrast, EP La Niña events are characterized by intensified upwelling conditions, favoring bloom-forming genera such as *Chaetoceros* spp. The Peruvian Andes receive seasonal precipitation, mainly in austral summer (January, February, and March), but the Peruvian coastal deserts remain dry except during EP El Niño events of sufficient magnitude (Ortlieb and Macharé, 1993; Wells, 1990). In contrast, La Niña events enhance the droughts that are characteristic of the region.

3. Methodology

The X-ray radiographies of the cores were carried out using an X-ray image-processing instrument (Migeon et al., 1999), and the elementary composition of the sediment was determined using the AVAATECH XRF core-scanner at the University of Bordeaux. Prior to analysis, the sediment surface of slabs carved from half-core sections was flattened and covered with Ultralene film to avoid desiccation during measurements, diminish surface roughness, and prevent contamination of the detector unit (Richter et al., 2006). XRF-measurements were conducted at two different tube voltages (10 and 30 keV) allowing for the determination of major elements associated with the biogenic (Silicon [Si]), organic (Bromine [Br]), and terrigenous fractions (e.g., Iron [Fe], Zirconium [Zr] and Titanium [Ti]). The analyses were performed at a high downcore resolution of 200 μm, thus enabling the capture of millimetric laminations based on their color (pictures), density (X-ray radiography), and elementary composition (XRF). These laminations were sampled individually, with respect to their shape in order to avoid the mixing of sediments of different age and composition.

For the diatom analysis, three slides were mounted per sample using the procedure described in Rathburn et al. (1997). Diatom identification was carried out using an Olympus BX-51 phase contrast microscope at a magnification of × 1000, following the counting rules described in Crosta and Koç (2007). A minimum of 300 valves were counted for each sample. Diatoms were identified at a species or species-group level, and the relative abundance of each species was determined as a fraction of the total quantity of diatom estimated in the sample. The identification of marine

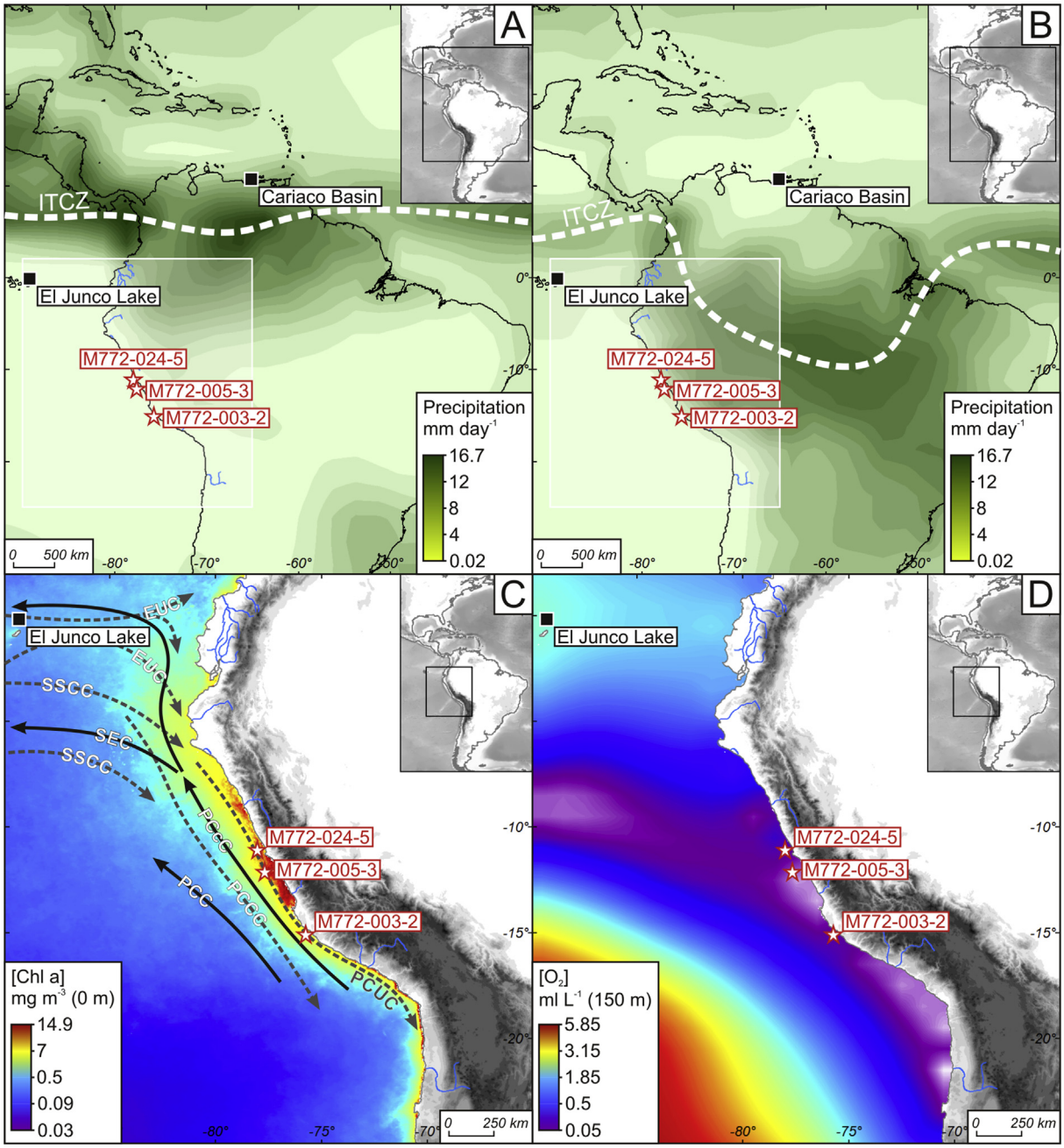

Fig. 1. A: Average boreal summer (June, July and August) precipitations and ITCZ location over 30 years (1980–2010). B: Average boreal winter (December, January, February) precipitations and ITCZ location over 30 years (1980–2010). Precipitation data are derived from NASA GPCP (http://iridl.ldeo.columbia.edu; Adler et al., 2003; Huffman et al., 2009). C: Chlorophyll a concentrations from Aqua MODIS averaged from 2002 to 2013 winters (http://oceancolor.gsfc.nasa.gov). Surface and subsurface currents are marked by solid black and dash gray lines, respectively. EUC: Equatorial Undercurrent; PCC: Peru–Chile Current; PCcC: Peru–Chile Coastal Current; PCCC: Peru–Chile Counter Current; PCUC: Peru–Chile Undercurrent; SEC: South Equatorial Current; SSCC: Southern Subsurface Counter Current (adapted from Mollier-Vogel et al., 2012). D: Annual oxygen concentrations at 150 m water depth, from World Ocean Atlas 1994 (http://iridl.ldeo.columbia.edu; Levitus and Boyer, 1994).

diatoms was based on a range of existing literature (Hasle et Syvertsen, 1996; Moreno et al., 1996; Sar et al., 2001, 2002; Sarno et al., 2005; Sundström, 1986; Sunesen et al., 2008), and the identification of brackish and freshwater diatoms was based on the work of Moreno et al. (1996).

We measured the nitrogen isotopic composition ($\delta^{15}N$) of the organic matter in the same samples as those prepared for the diatom census counts. Nitrogen isotope ratios ($\delta^{15}N$) were determined on 8–15 mg of dried, ground, and homogenized bulk sediment using a Carlo-Erba CN analyzer 2500 interfaced with a Micromass Isoprime mass spectrometer. The internal consistency of our measurements was continuously checked using several calibrated laboratory standards. Their reproducibility, based on in-house and international standard replicates, was ±0.30‰.

We performed a continuous wavelet transform on our records using a Matlab program to estimate the frequency of the most significant variations (Chatfield, 1989; Jenkins and Watts, 1968; Lau and Weng, 1995). To this end, we used a script written by Christopher Torrence (1998). The 90% significance of the signal was determined using a red-noise background spectrum (Gilman et al., 1963). In addition, we estimated temporal differences in the variability of our record. To this purpose, we used a band-pass Gaussian

filter on evenly-spaced data with the Macintosh AnalySeries program (Paillard et al., 1996).

4. Core description and stratigraphy

4.1. Core description

Trigger cores M772-024-5, M772-005-3, and M772-003-2 were respectively retrieved at 11°S (longitude: 78°W, depth: 210 m), 12°S (longitude: 77°39′W, depth: 210 m) and 15°S (longitude: 75°44′W, depth: 271 m) during Meteor cruise M-772 in 2008. All cores were located on the edge of the Peruvian shelf, within the OMZ. They were all positioned south of 10°S, where oxygen depletion is the most intense. Very low seafloor oxygen concentrations in this area (Mollier-Vogel, 2012) make it suitable for the preservation of laminations. The sediments were composed of laminations that appeared alternatively light and dark on the X-ray radiographies. The light laminations contained dark olive to olive clays or silty clays; high quantities of micro-fossils, dominated by diatom frustules; and low quantities of dense terrigenous material, according to XRF measurements. In contrast, the dark laminations were characterized by dark olive to gray silty clays or silts, lower quantities of microfossils, and higher quantities of terrigenous material. The darker laminations were therefore denser than the lighter laminations and appeared darker on the X-ray radiographies.

In addition to laminations, we identified four main sedimentary units, labeled Units I to IV from top to bottom. The units were determined according to the predominance of either light or dark laminations on the X-ray radiographies (Fig. 2). Laminations of both types could be seen within one unit. Unit I was dominated by light laminations, while Unit II was composed of darker laminations. Both units were present in all cores. Core M772-003-2 displayed two other units besides Units I and II. Unit III was dominated by light laminations, while Unit IV was composed of dark laminations. All the cores showed the same succession of units, with a unit that was dominated by light laminations at the top (Unit I), followed by one that was dominated by dark laminations (Unit II). The longest core (M772-003-2) displayed another dark/light pair of units, showing that the succession of dark and light units had been repeated in the past. The repetition of the same units in all the cores suggests that similar conditions prevailed throughout the Peruvian Upwelling System at any given moment. Previous studies on sediments from the Peruvian margin confirm this assumption, indicating similar sources for terrigenous particles deposited off the coast of southern Peru (Krissek et al., 1980; Scheidegger and Krissek, 1982). We can thus assume that sedimentary units of the same color were deposited at the same time in all three core locations. We also observed similar trends in the Si/Fe signals of the three cores (Fig. 2). Similar Si/Fe ratios suggest that the composition of each unit is the same in all three cores.

4.2. Core chronology

The age model of core M772-003-2 was established through the combination of ^{210}Pb and ^{14}C analysis (Table 1, Fig. 3). We then correlated cores M772-005-3 and M772-024-5 to the reference

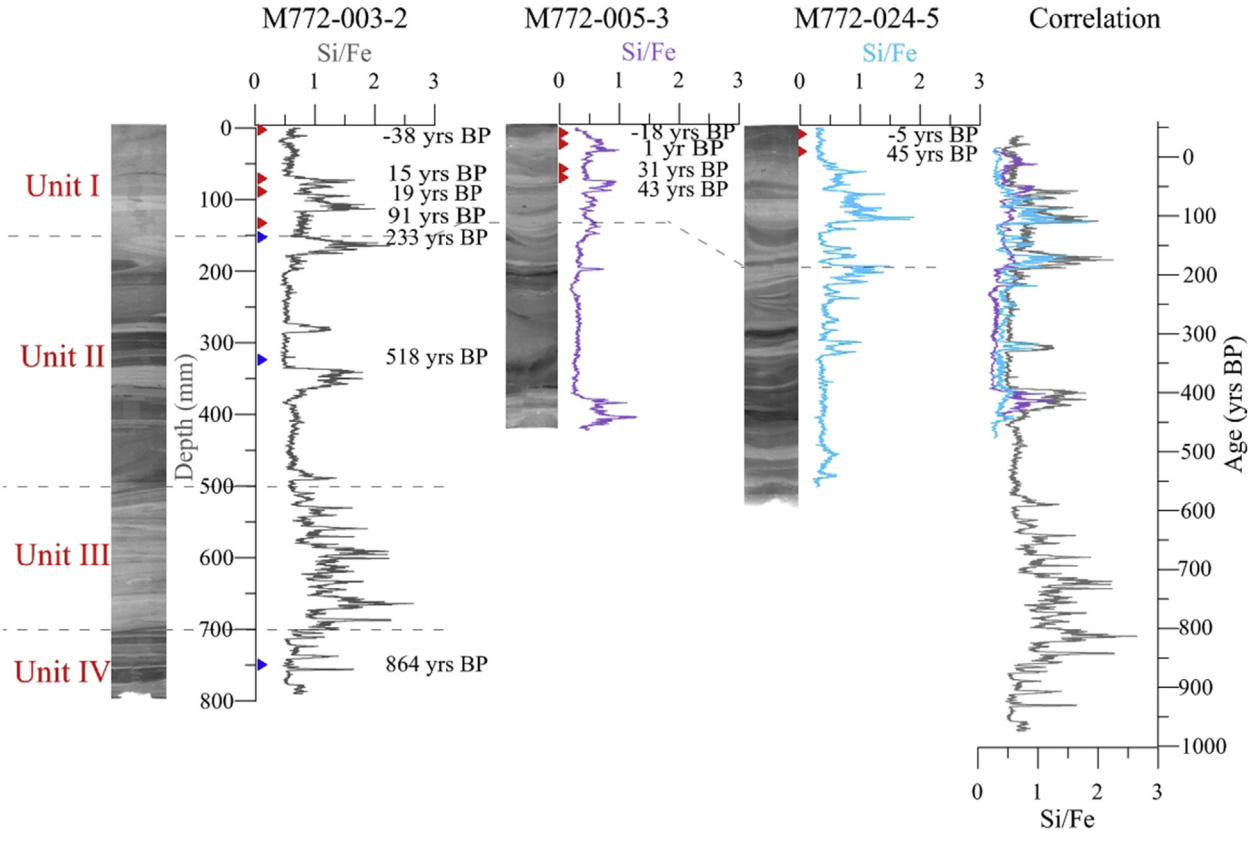

Fig. 2. Chronology of the three cores. The age model of trigger core M772-003-2 is based on ^{210}Pb measurements (red triangles) and ^{14}C analyses (blue triangles). The two other trigger cores were correlated with core M772-003-2 through the identification of their sedimentary units and the comparison of their Si/Fe ratios, as well as by taking into consideration the ^{210}Pb ages of their most recent sections. The ages of the limits of the units on core M772-003-2 are based on the age model shown on Fig. 3. (For interpretation of the references to color in this figure legend, the reader is referred to the web version of this article.)

Table 1
Ages available on the trigger cores.

Core	Depth (cm)	Method	Radiocarbon age (years BP)	Error (years)	2σ (years BP)	Calibrated age (years BP)	Calendar age (AD)	Error (years)
M772-003-2	0	^{210}Pb	–	–	–	–	1988	±10
	2	^{210}Pb	–	–	–	–	1982	±10
	7	^{210}Pb	–	–	–	–	1935	±10
	9	^{210}Pb	–	–	–	–	1931	±10
	13	^{210}Pb	–	–	–	–	1859	±10
	15	^{14}C	715	±30	49–418	233.5	1716.5	±278
	32	^{14}C	1035	±30	266–271	518.5	1431.5	±278
	75	^{14}C	1390	±30	603–1125	864	1086	±278
M772-005-3	0	^{210}Pb	–	–	–	–	1968	±10
	2	^{210}Pb	–	–	–	–	1949	±10
	5	^{210}Pb	–	–	–	–	1919	±10
		^{210}Pb	–	–	–	–	1907	±10
M772-024-5	0	^{210}Pb	–	–	–	–	1955	±10
	2	^{210}Pb	–	–	–	–	1905	±10

core M772-003-2, which spans the longest time period and for which the age model is better constrained.

A $^{210}Pb_{xs}$ profile was determined for each core as the difference between the total (^{210}Pb) and supported (^{226}Ra) activities in the sediment, measured using low-background high-efficiency gamma spectrometry (Schmidt et al., 2013). We here selected the CIC model (Constant Initial Concentration; Robbins and Edgington, 1975), stating that the initial activity of $^{210}Pb_{xs}$ remains the same for all samples within a same core. The CIC model enables to take into account past changes in sedimentation, which are highly probable in our cores given the strong changes in density observed on the X-ray images. The age of each point is thus calculated using the following equation:

$$t = (1/\lambda) * \ln(A_0/A)$$

t: age of the sample (in years)
λ: decay constant (λ = 0.031 year^{-1} for ^{210}Pb)
A_0: $^{210}Pb_{xs}$ activity in mBq g^{-1} measured on the fluffy layer (contemporaneous to the retrieval date of the trigger cores) on top of the multi-core retrieved at the same place as the trigger core
A: $^{210}Pb_{xs}$ activity in mBq g^{-1} measured on the sample.

Three radiocarbon ages were obtained, only on core M772-003-2, by Accelerator Mass Spectrometry on humic acids extracted from the organic matter on dried and homogenized sediment samples

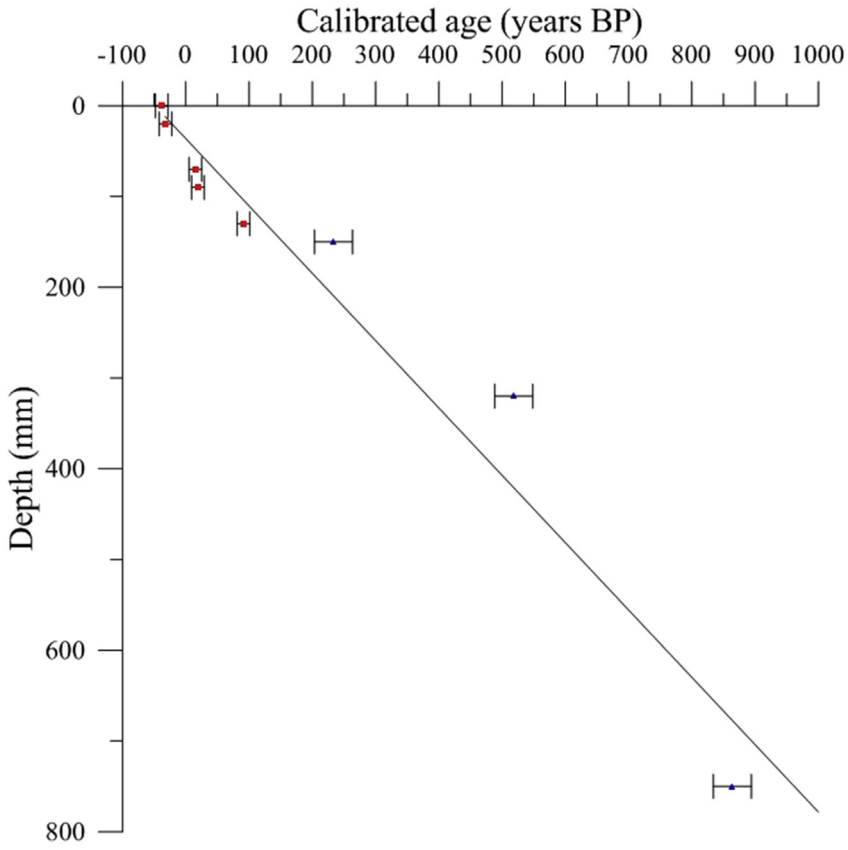

Fig. 3. Age model of trigger core M772-003-2. The blue triangles indicate the ^{14}C ages while the red squares represent the ^{210}Pb ages. The horizontal bars represent the error on the age measurements. The line indicates the linear age model following the equation: Age (years BP) = 1.2782*Depth (mm) − 35.582. (For interpretation of the references to color in this figure legend, the reader is referred to the web version of this article.)

(Table 1). The radiocarbon ages were corrected, considering a mean reservoir age of 511 ± 278 years (Ortlieb et al., 2011) and calibrated using the Marine13 calibration curve program (Reimer et al., 2009; Stuiver and Reimer, 1993; http://calib.qub.ac.uk/marine/). Individual sample ages on core M772-003-2 were calculated by using the linear regression on the ^{210}Pb and ^{14}C control points, following the equation:

$$\text{Age (years BP)} = 1.2782*\text{Depth (mm)} - 35.582$$

The correlation of cores M772-005-3 and M772-024-5 on core M772-003-2, through their Si/Fe records, representative of biogenic silica (opal), enabled to assign an age model to the two shorter cores on which no radiocarbon dates were available (Fig. 2). The age models obtained via this method are in good agreement with the ages calculated by the ^{210}Pb activities measured on the upper part of cores M772-005-3 and M772-024-5 (Table 1).

5. Results and discussion

Based on a multiproxy approach, the laminated sediments from the Peruvian continental shelf allowed us to trace long-term variations and changes in the multidecadal variability of terrigenous sedimentation, productivity, and OMZ intensity.

5.1. Sedimentation rates and age span of the laminae

The trigger cores measure 50 cm (M772-024-5), 43.2 cm (M772-005-3) and 80.2 cm (M772-003-2) respectively, which cover 537, 475 and 1025 years. Their mean sedimentation rate is thus equal to 0.97 mm/year (M772-024-5), 0.91 mm/year (M772-005-3) and 0.78 mm/year (M772-003-2). These values are in agreement with the range in sedimentation rates observed on the Peruvian margin between 10 and 15°S (0.4–3.3 mm/year; review in Gutiérrez et al., 2009).

We identified 87, 66 and 145 millimetric laminations in cores M772-024-5, M772-005-3 and M772-003-2, respectively. Their respective age models allowed us to estimate that one lamination represents six to eight years, probably deposited over several years during which similar conditions prevailed in the study area. The sampling thus reaches the multiannual timescale but does not allow tracing individual El Niño or La Niña events.

5.2. Long-term variations in rainfall, productivity, and denitrification

Following previous studies (Rein et al., 2004, 2005), we considered iron (Fig. 4a) as a tracer of the lithogenic fraction of the sediment. Even though iron could be released from sediments under the reducing conditions typical of OMZs (Scholz et al., 2014), this phenomenon is not the main driver of Fe downcore variations in our sediment cores since Fe varies in parallel with zirconium (Zr) (Fig. 4b) and titanium (Ti) (Fig. 4c), which are not sensitive to redox conditions. Lithogenic particles could be brought to our study site either through wind transport or runoff. The first hypothesis can be ruled out since the contribution of aeolian dust to sedimentation is small compared to riverine sediments on the Peruvian margin (Scheidegger and Krissek, 1982). In addition, the mineral particles observed in a sediment core at 12°S, i.e. at the same area as core M772-005-3, are too angular to be transported by wind (Sifeddine et al., 2008). Fe, Zr and Ti contents are thus representative of runoff changes on the Peruvian coast, driven by rainfall over the nearby continent.

Our records showed three main periods over the last millennium. Low terrigenous contents were generally observed between 850 and 650 years BP and between 200 years BP and the present, while higher terrigenous contents were generally recorded between 1000 and 850 years BP and between 650 and 200 years BP (Fig. 4a). The three terrigenous records in core M772-003-2 thus indicate higher precipitations during the LIA with several shorter humid intervals during the MWP and the CWP. Conversely, drier conditions are inferred for most of the MWP and CWP.

The increase in precipitation observed off the Peruvian coast during the LIA, compared to the MWP and CWP, could have been caused either by a southward shift of the ITCZ (Sachs et al., 2009) or by sustained El Niño-like mean conditions (Horel and Cornejo-Garrido, 1986). We observed a clear negative correlation between the Fe content of core M772-003-2 from the Peruvian shelf (Fig. 4a), and the Ti content of core ODP1002C from the Cariaco Basin (Fig. 4d), supporting the idea of a southward migration of the mean position of the ITCZ during the LIA. The ITCZ currently sweeps the Cariaco Basin in boreal summer and passes above northwestern South America in boreal winter, in response to the northward migration of maximum received solar radiative energy (Garreaud et al., 2009). A southward migration of the mean ITCZ position modifies the distribution of precipitation over the equatorial band, leading to more humid conditions to the south and drier conditions to the north. Conversely, a northward migration of the mean ITCZ position produces more humid conditions in the Cariaco Basin and more arid conditions in northwestern South America. This phase opposition between the Cariaco Basin and northwestern South America has already been observed for the Holocene and the last deglaciation (Mollier-Vogel et al., 2013). Southward movements of the ITCZ have been observed in periods of decreased summer insolation in the northern hemisphere, e.g. during the Late Holocene (Haug et al., 2001), leading to the hypothesis of orbitally-driven shifts of the ITCZ (Cruz et al., 2005). Cooler conditions in the northern hemisphere lead to stronger north–south temperature gradients, which strengthen cross-equatorial heat transport and lead to enhanced northern trade winds (Wang et al., 2007). Similar shifts have been observed at the millennial timescale however, with southward movements taking place during Heinrich events and Dansgaard–Oeschger stadials (Leduc et al., 2009). These events all correspond to enhanced northern hemisphere cooling. The proposed mechanism is the same at this timescale, but northern hemisphere cooling is thought to be caused by reduced Atlantic Meridional Overturning Circulation (AMOC; McManus et al., 2004). Finally, evidence has been published for a southward shift of the ITCZ during the LIA (Sachs et al., 2009), concurrently with reduced AMOC (Lund et al., 2006). Our record appears to have been mainly influenced by the ITCZ at the centennial timescale since it was negatively correlated to northern hemisphere records (Haug et al., 2001), as predicted when the ITCZ is the main influence (Leduc et al., 2009). However, the M772-003-2 Fe, Zr and Ti records do not correspond to the Ti record from the Cariaco Basin at shorter timescales, suggesting that other forcing mechanisms were also involved.

Another possible mechanism leading to higher precipitation in northwestern South America is the weakening of the Walker circulation, which is conditioned by the east–west pressure gradient in the Pacific Ocean (Bjerknes, 1969). Enhanced Walker circulation favors La Niña events, expressed as cold SSTs in the eastern equatorial Pacific Ocean and warm SSTs in the western equatorial Pacific Ocean (Julian and Chervin, 1978). La Niña events are thus characterized by stronger east–west SST gradients. We here consider that the east–west SST gradient indicates La Niña-like mean conditions when it is above the modern mean gradient (Conroy et al., 2010). The record by Conroy et al. (2010) suggests that the east–west SST gradient (Fig. 4e) was higher than its modern mean value over the MWP, while it was lower than its mean value during the LIA. Even

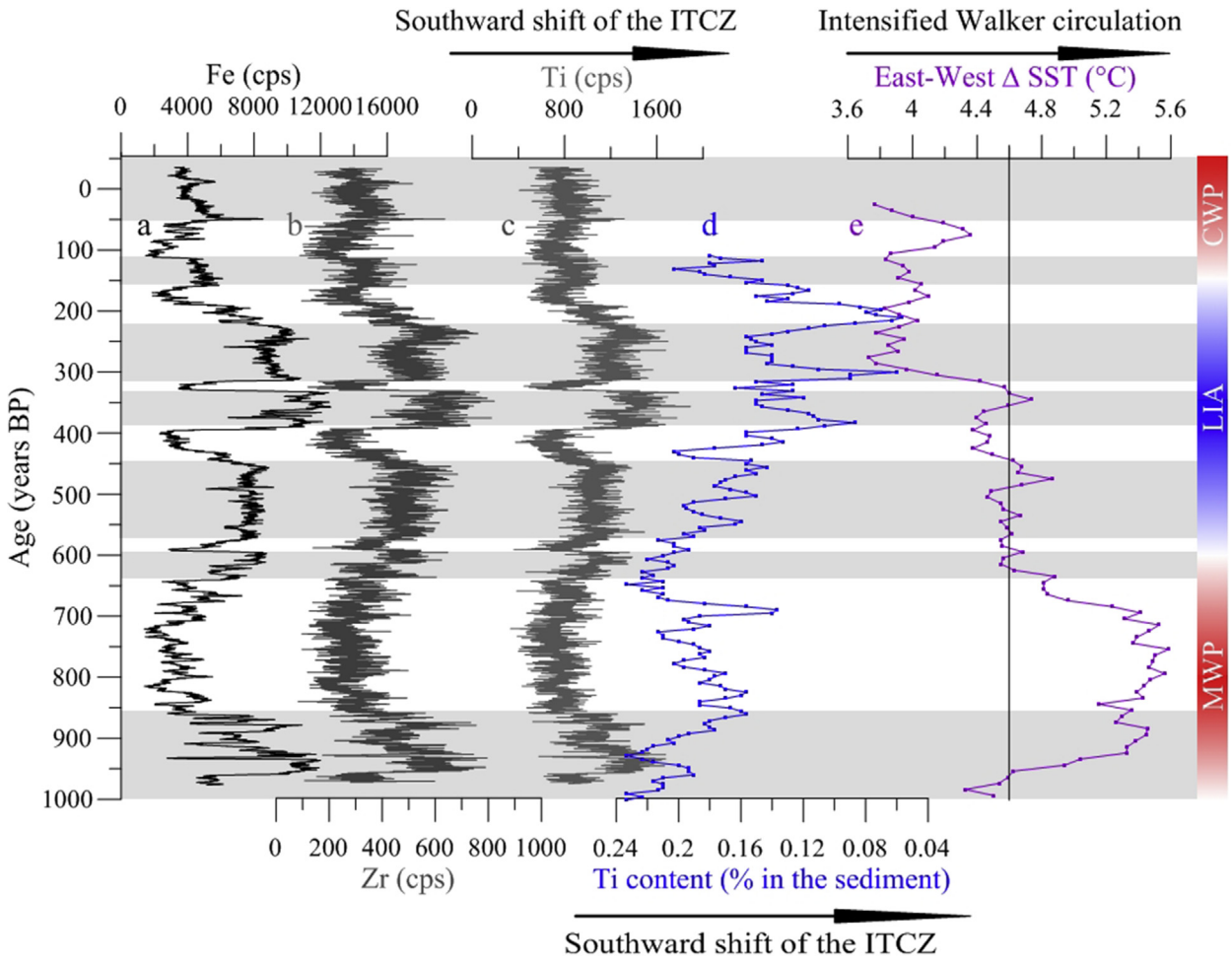

Fig. 4. Comparison between precipitation proxies in core M772-003-2 and from around northern South America: (a) iron, (b) zirconium and (c) titanium contents measured in core M772-003-2, 15°S off the Peruvian coast (this study); (d) titanium content in marine core ODP1002C, in the Cariaco Basin, 10°N (Haug et al., 2001); (e) east–west SST gradient in the equatorial Pacific (Conroy et al., 2010). The gray shaded areas indicate humid intervals in coastal Peru inferred from our records. The vertical line indicates the modern mean east–west SST gradient in the equatorial Pacific (Conroy et al., 2010). The MWP, the LIA and the CWP were defined based on the combination of the studies by Graumlich (1993), Grove (1988), Lamb (1985), and Stuiver et al. (1995). The blue and red areas are shaded to take into account the discrepancies between the definitions. (For interpretation of the references to color in this figure legend, the reader is referred to the web version of this article.)

though this record would gain to be supported by other records of the zonal SST gradient, it may indicate that the MWP was dominated by La Niña-like mean conditions, while El Niño-like mean conditions prevailed during the LIA. More records of the zonal SST gradient at the centennial timescale are needed to confirm these results. Increased Fe contents off Peru (Fig. 4a) yet suggests El Niño-like mean conditions between 1000 and 850 years BP, contrasting with the upper phase of the MWP, dominated by La Niña-like mean conditions. This humid period within the early MWP coincides with a dry period in the Cariaco Basin (Fig. 4d) and reduced zonal SST gradients in the Pacific Ocean (Fig. 4e). Our records thus support the reduction of the Walker cell at the MWP–LIA boundary. We note, however, that our data demonstrates low mean precipitation during the CWP, while the east–west SST gradient, which is well below its modern mean value (Fig. 4e), argues for El Niño-like mean conditions over this period. This may indicate that other processes, such as changes in the background state in response to a secular positive trend in tropical SST (Li et al., 2013), may have counterbalanced the reduction in the Walker circulation since AD 1800.

The investigation of the biogenic fraction preserved down-core allows assessing the impact of these climate changes on local productivity. C/N ratios measured on these cores (Fleury, 2015) were all between 8 and 13, with mean values around 9.29, 10.1 and 8.79 for cores M772-024-5, 005-3 and 003-2 respectively, showing values typical of oceanic derived organic matter (Meyers, 1997). A similar predominance of marine organic matter was observed in surface sediments from the Peruvian margin (Mollier-Vogel, 2012) as well as on all sediment cores from the Peruvian margin (Diaz-Ochoa et al., 2009; Gutiérrez et al., 2009; Mollier-Vogel, 2012; Morales et al., 2006; Wolf, 2002).

The biogenic elements were normalized to iron, as suggested for this region by Agnihotri et al. (2008). Br/Fe ratios were high during the MWP, decreased during the LIA, and increased again during the CWP (Fig. 5c, g and k). The MWP thus appears to have been a productive period, the LIA a period of lower productivity, and the CWP a period with moderate productivity. These geochemical data were also compared to diatom countings. The genus *Chaetoceros Hyalochaete* spp, which dwells in nutrient-rich upwelling cells (Abrantes et al., 2007) and produces resting spores in conditions of nutrient depletion due to high utilization, was the dominant diatom group in our three cores. We observed higher abundances of *Chaetoceros* resting spore during the MWP and CWP (Fig. 5b, f, and j), indicating high nutrient utilization during these periods. High nutrient utilization was probably induced by strong diatom blooms,

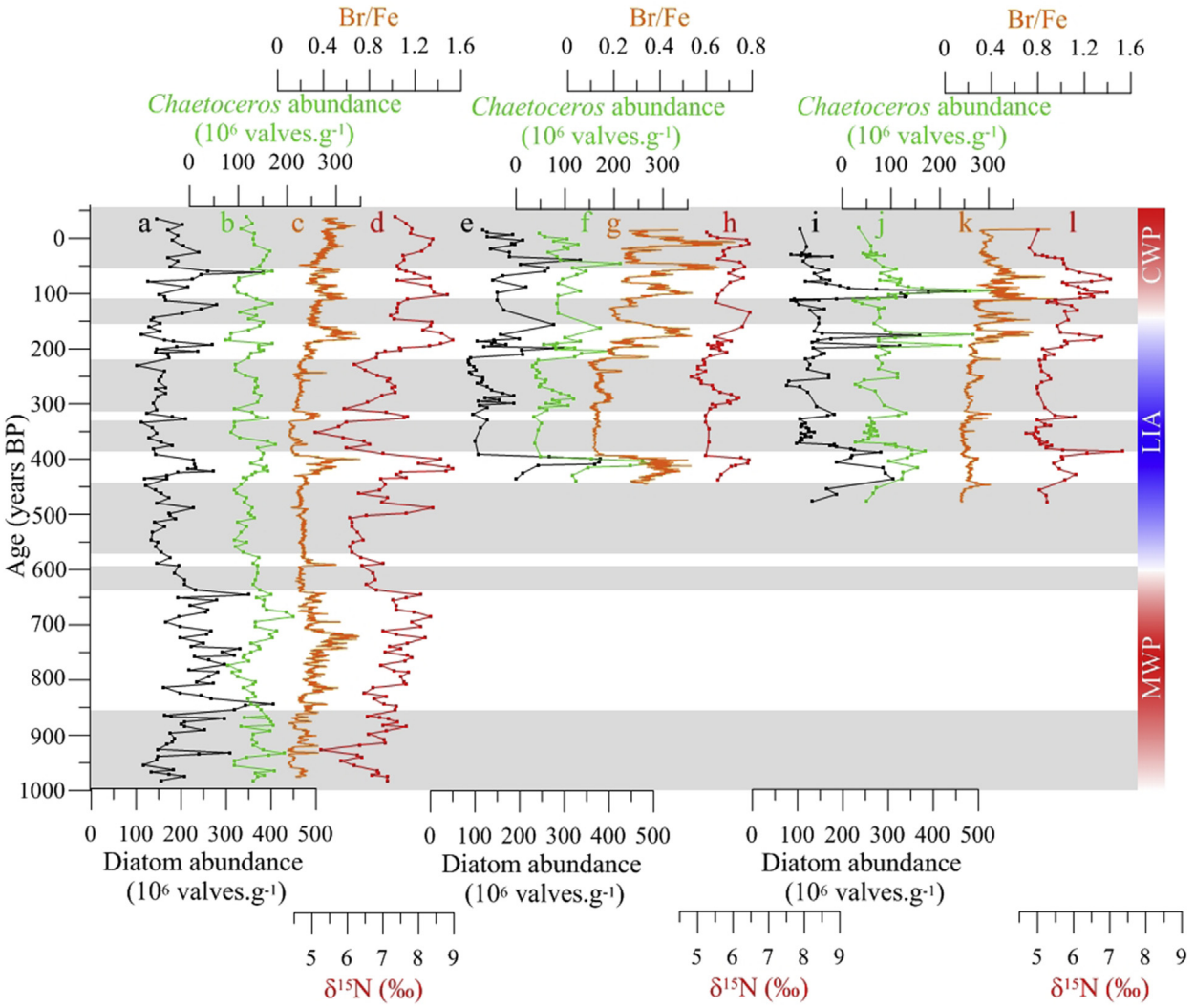

Fig. 5. Records of productivity and nitrogen isotopes in cores M772-003-2 (15°S, plots a to d), M772-005-3 (12°S, plots e to h) and M772-024-5 (11°S, plots i to l). Total diatom abundances are represented in black (a, e and i), *Chaetoceros* resting spore abundances in green (b, f and j), Br/Fe ratios in orange (c, g and k), and $\delta^{15}N$ values in red (d, h and l). The gray shaded areas indicate the intervals with the lowest productivity, which coincide with the humid periods identified on Fig. 4. (For interpretation of the references to color in this figure legend, the reader is referred to the web version of this article.)

as suggested by the concurrence of high abundances of *Chaetoceros* resting spores with high total diatom abundances (Fig. 5a, e and i). Low productivity in the eastern tropical Pacific currently occurs during El Niño events (Pennington et al., 2006; Montecino and Lange, 2009), and as such, our productivity records indicate that both the MWP and the CWP were dominated by La Niña-like mean conditions, while the LIA was dominated by El Niño-like mean conditions in agreement with interpretations drawn from the terrigenous proxies.

We observed that all productivity proxies varied in phase with $\delta^{15}N$ (Fig. 5d, h and l). Nitrogen isotopes are considered to be a tracer of denitrification within the core of the Peruvian oxygen minimum zone, as demonstrated in previous studies (Agnihotri et al., 2006, 2008; Gutierrez et al., 2009; Mollier-Vogel et al., 2012), with greater denitrification being recorded by higher $\delta^{15}N$ values. The same conclusions have been obtained for other sedimentary $\delta^{15}N$ records from similar oceanographic settings, e.g., the Eastern Tropical North Pacific OMZ, the Arabian Sea OMZ and further south off Chile (Altabet et al., 1995, 2002; De Pol-Holz et al., 2006; Galbraith et al., 2008; Ganeshram et al., 1995; Hendy and Pedersen, 2006; Pichevin et al., 2007; Robinson et al., 2007; Thunell and Kepple, 2004). Our data thus indicate that $\delta^{15}N$ mean values were lower over the LIA than the CWP or MWP. Denitrification was thus reduced over the LIA compared to the other periods. All other $\delta^{15}N$ records from the Peruvian and north Chilean shelves display similar trends (Gutiérrez et al., 2009; Vargas et al., 2004, 2007). These changes have been observed regionally, suggesting a common climatic forcing, behind productivity (oxygen demand) changes. This forcing is probably ENSO, since denitrification decreases today during El Niño events in which the subsurface waters of the Peruvian OMZ are better oxygenated (Gutiérrez et al., 2008). These reoxygenation episodes have been interpreted as the result of increased equatorial dynamic height during El Niño events. This increase, which is caused by stronger and more frequent Kelvin waves (e.g. Kessler and McPhaden, 1995), leads to a deepening of the thermocline and a downward shift of the OMZ. The equatorial dynamic height controls both the position and the intensity of the OMZ, since bottom water oxygenation increases during El Niño events (Gutiérrez et al., 2008). Decreased $\delta^{15}N$ values thus indicate lower oxygen deficiency in the OMZ (lower oxygen demand) and/or a deepening of the OMZ, which is characteristic of El Niño-like mean conditions. Our records suggest that oxygen deficiency was

weaker in the OMZ over the LIA, while it was stronger during the other periods. A weakening of the oxygen depletion was also observed on the Peruvian and Chilean shelves during the LIA in studies of redox-sensitive elements (Diaz-Ochoa et al., 2011; Gutiérrez et al., 2009). Increased oxygenation within the OMZ over the LIA supports the idea of prevailing El Niño-like mean conditions during this period.

We can sum up our observations on long-term changes by dividing the last millennium into three main periods. The MWP and CWP have displayed drier conditions, stronger productivity, and weaker oxygenation, with the ITCZ located in its modern position or further north. The first three conditions are typical of La Niña events (Philander, 1990; Wells, 1990), suggesting dominant La Niña-like mean conditions over these two periods. Contrasting conditions have been observed over the LIA, with increased rainfall, decreased productivity, and increased oxygenation, along with an ITCZ displaced to the south. The LIA thus appears to have been dominated by El Niño-like mean conditions. Nevertheless, our proxies also display multidecadal variability in all the periods, suggesting that multidecadal variations can occur under different mean conditions.

5.3. Changes in multidecadal variability

The long-term changes in precipitation in northwestern South America and the oceanic productivity off the Peruvian coast inferred from our records were interrupted by short-term variations (Figs. 4 and 5), the timeframes of which were quantified using a wavelet transform. This analysis was performed on the M772-003-2 Si/Fe record (Fig. 6b), which offers a sub-annual resolution over the last millennium. Significant periodicities between 30 and 50 years prevailed throughout the record (Fig. 6a) but were more pronounced over the last 450 years. Significant shorter periodicities, between 15 and 20 years, were evident during the early MWP, the LIA and late CWP. Such results indicate that multidecadal variability was present during the three climatic intervals of the last millennium. Following the wavelet results, Si/Fe ratios were filtered for periods of between 30 and 50 years (frequency center = 0.027 and bandpass width = 0.007) to better evidence the variance present in the record.

The filtered Si/Fe record displays persistently strong multidecadal variability over the last 450 years (Fig. 6c), with maxima between 400 and 300 years BP and between 200 and 50 years BP. Two other intervals with strong multidecadal variations are observed between 850 and 775 years BP and between 700 and 550 years BP. These results support the idea of strong multidecadal variability over the LIA and the CWP as already evidenced in North American drought records (Li et al., 2011). However, our results indicate strong multidecadal variations in several periods of the MWP as well while North America drought records suggested a reduction in multidecadal variance over the MWP (Li et al., 2011). Observing multidecadal variations as strong in the MWP as in the LIA and the CWP, regardless of the mean conditions prevailing, contradicts the hypothesis of the multidecadal pacing of ENSO by the mean state of the Pacific Ocean, proposed by Li et al. (2011). Furthermore, the earliest maximum in multidecadal variance (850–775 years BP) occurred over a period of high zonal SST gradient (Conroy et al., 2010, Fig. 6d) while all the other maxima took place under conditions of reduced zonal SST gradient (Fig. 6d), i.e. independently of the mean state of the Pacific Ocean. We thus investigate alternative causes for multidecadal variations by comparing our record to the reconstructions of possible forcing mechanisms, i.e., the meridional circulation and North Atlantic Oscillation, solar irradiance and volcanic activity.

The current period of increased multidecadal variability began 450 years ago, when the North Atlantic Oscillation (NAO) index

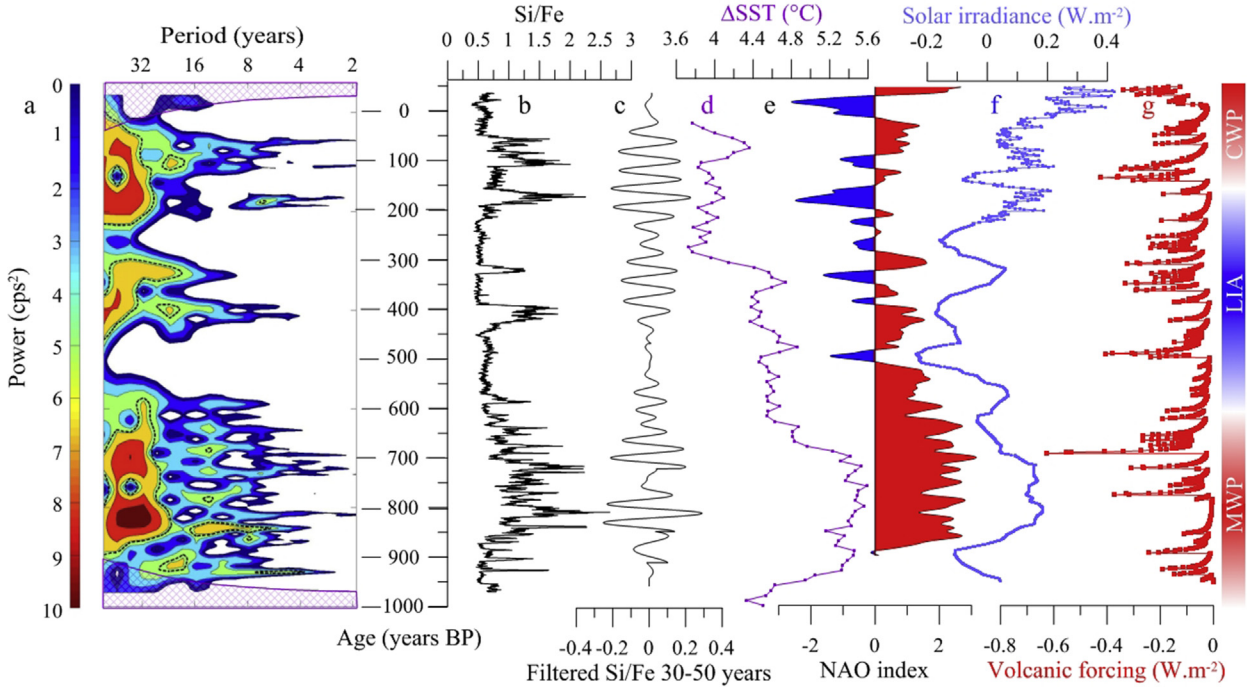

Fig. 6. Comparison of the Si/Fe record in core M772-003-2 along with internal and external forcing mechanisms. (a) wavelet power spectrum of the Si/Fe record (this study); (b) the Si/Fe ratio; (c) the Si/Fe record filtered with a Gaussian band-pass filter (this study) for periods between 30 and 50 years; (d) east–west SST gradient in the equatorial Pacific (Conroy et al., 2010); (e) the North Atlantic Oscillation index reconstructed from speleothems and tree-rings (Trouet et al., 2009); (f) solar activity and (g) volcanic forcing on the Earth's radiative budget (Mann et al., 2005). The power has been scaled by the global wavelet spectrum. The cross-hatched region is the cone of influence, where zero padding has reduced the variance. Black contour is the 90% significance level, using a red-noise background spectrum.

started oscillating between positive and negative phases, possibly with a dominance of the negative phase (Fig. 6e; Trouet et al., 2009). This observation might suggest an interaction between the Atlantic and the Pacific Ocean, even though more records of the NAO are needed to settle this hypothesis. Modern observations show a similar concurrence of strengthened ENSO-like multidecadal variability with negative NAO indices (Delworth and Mann, 2000) between AD 1965 and 1990. The NAO also impacts the Atlantic Meridional Oceanic Circulation, which may in turn affect the ENSO-like multidecadal variability. Indeed, previous studies indicated that a negative NAO index weakens the AMOC (Curry et al., 1998) through the weakening of North Atlantic water inflow into the Nordic seas (Sicre et al., 2008).

Model experiments suggest that a strong decrease in AMOC conducts to a reorganization of northern hemisphere atmospheric circulation. Northern trade winds are intensified in the North Atlantic, leading to the southward displacement of the ITCZ in this region (Saenger et al., 2009). The reduction of the AMOC also results in the cooling of the tropical Atlantic Ocean and the Caribbean Sea (Timmermann et al., 2007) and generates an anticyclonic circulation over the Caribbean Sea (Xie et al., 2007). Such a process results in anomalously cold and dry northern trade winds over the North Pacific (Wu et al., 2005). The northeastern tropical Pacific also becomes cooler, enhancing northern trade winds over the Pacific Ocean and causally cooling it. The ITCZ subsequently shifts southward in the Pacific Ocean, which warms the southeastern Pacific. The resulting reduced gradient between the northeastern and southeastern Pacific reduces the annual cycle of sea surface temperatures (i.e. the seasonal variations driven by the ITCZ) and enhances ENSO activity. Similarly, increased ENSO-like multidecadal variability was observed during the negative phase of the Atlantic Multidecadal Oscillation between AD 1965 and 1990 (Dong et al., 2006). This multidecadal oscillation shifts to a negative index in periods of decreased AMOC and negative NAO (Delworth and Mann, 2000), inducing cooling in the North Atlantic and warming in the South Atlantic (Knight et al., 2005) as well as a southward shift of the ITCZ (Knight et al., 2006). A mechanism similar to the one proposed by Timmermann et al. (2007) might thus enhance multidecadal ENSO-like activity in periods of North Atlantic cooling. Our record might support this idea through the concurrence of the period of increased multidecadal variability with a period of reduced NAO index (Fig. 6e).

The MWP maxima in multidecadal variability (between 850 and 775 years BP and between 700 and 550 years BP) conversely occurred during periods of sustained positive NAO, which could go against the hypothesis of multidecadal variability triggered by a negative phase of the NAO. However, we note that the NAO may have been more variable than suggested by Trouet et al. (2009). More recent studies provided evidence for the occurrence of two intervals of negative NAO conditions. The first period occurred around AD 1120 (825 years BP) and is supported by indices of a wet phase in Morocco (Wassenburg et al., 2013) and the Iberian Peninsula (Abrantes et al., 2011; Moreno et al., 2012). The second interval took place around AD 1400 (550 years BP), as shown by the NAO reconstructions from West Greenland (Olsen et al., 2012). We observe strong multidecadal variability on the Peruvian margin around 800 years BP (AD 1150) and 550 years BP (AD 1400), which may further suggest that NAO variability was stronger than indicated by Trouet et al. (2009) if the teleconnection between the North Atlantic and the Pacific Ocean was the same over the MWP as for younger intervals.

The two intervals of increased multidecadal variability observed during the MWP (between 850 and 775 years BP and between 700 and 550 years BP; Fig. 6c) occurred when decreases in solar irradiance (Fig. 6f) were combined with increased volcanic activity (Fig. 6g). Minima in solar activity are thought to be responsible for minima in northern hemisphere temperatures over the last millennium (Mann et al., 1999). Strong multi-decadal variations in productivity off Peru may thus be favored by northern hemisphere cooling. The strong impact of volcanism on ENSO activity has already been proposed by Li et al. (2013), whereby strong eruptions lead to anomalous cooling in the central-eastern tropical Pacific the year of the eruption (La Niña-like conditions), followed by anomalous warming the following year (El Niño-like conditions). Our results suggest that solar irradiance and volcanic activity may contribute to strong multidecadal variability.

6. Conclusion

A multi-proxy approach on laminated sediments from the Peruvian shelf has allowed the reconstruction of long-term changes in rainfall, productivity, and denitrification, as well as their multidecadal variations. The long-term changes observed support the division of the last millennium into a Medieval Warm Period dominated by arid conditions (La Niña-like mean conditions), a Little Ice Age dominated by humid conditions (El Niño-like mean conditions) and a Current Warm Period dominated again by La Niña-like mean conditions. This centennial-scale division into three phases is driven by the latitudinal migrations of the ITCZ, a northward migration of the ITCZ generating La Niña-like mean conditions off Peru during the MWP and the CWP while El Niño-like mean conditions are caused by a southward migration of the ITCZ over the LIA. Pervasive multidecadal changes in productivity were observed over the last millennium independently of the mean climate state. The multidecadal variance in our records was stronger over the last 450 years, when the reconstruction of the NAO index suggests an oscillation between positive and negative phases. Our records also suggest that maxima in variance could be triggered by the combined action of solar activity and repetitive volcanic eruptions. Further investigations are needed to test the hypothesis of a link between NAO and multidecadal ENSO-like activity in eastern Pacific. More records of the NAO are needed to allow for a better comparison with records of ENSO-like activity, whereby model runs under the climatic conditions prevailing over the MWP and the LIA could be used to check whether the teleconnection proposed by Timmermann et al. (2007) also applies to these periods or is restricted to modern conditions.

Acknowledgments

We thank Sabine Schmidt for her expertise and help on ^{210}Pb analysis. Pascal Lebleu and Olivier Ther provided us with help in carrying out X-ray radiographies and extracting sediment slabs. Vincent Marieu, Melanie Moreau, and Philippine Campagne helped us with Matlab. We thank Jean-Pascal Dumoulin and Christophe Moreau from the CEA in Gif-sur-Yvette for performing a radiocarbon analysis on our samples. Sarita Jannin revised the language. We thank two anonymous reviewers for their comments that help improving the manuscript. The research leading to these results received funding from the European Union's Seventh Framework Programme (FP7/2007–2013) under Grant 243908, “Past4Future, Climate change—Learning from the past climate.” This is a Past4Future contribution.

References

Abrantes, F., Lopes, C., Mix, A., Pisias, N., 2007. Diatoms in Southeast Pacific surface sediments reflect environmental properties. Quat. Sci. Rev. 26, 155–169. http://dx.doi.org/10.1016/j.quascirev.2006.02.022.

Abrantes, F., Rodrigues, T., Montanari, B., Santos, C., Witt, L., Lopes, C., Voelker, A.H.L., 2011. Climate of the last millennium at the southern pole of the

North Atlantic Oscillation: an inner-shelf sediment record of flooding and upwelling. Clim. Res. 48, 261–280. http://dx.doi.org/10.3354/cr01010.
Adler, R.F., Huffman, G.J., Chang, A., Ferraro, R., Xie, P.P., Janowiak, J., Rudolf, B., Schneider, U., Curtis, S., Bolvin, D., Gruber, A., Susskind, J., Arkin, P., Nelkin, E., 2003. The version-2 Global Precipitation Climatology Project (GPCP) monthly precipitation analysis (1979–present). J. Hydrometeorol. 4 (6) doi: 10.1175/1525-7541(2003)004<1147:TVGPCP>2.0.CO;2.
Agnihotri, R., Altabet, M.A., Herbert, T.D., 2006. Influence of marine denitrification on atmospheric N_2O variability during the Holocene. Geophys. Res. Lett. 33 (13), L13704. http://dx.doi.org/10.1029/2006GL025864.
Agnihotri, R., Altabet, M.A., Herbert, T.D., Tierney, J.T., 2008. Subdecadally resolved paleoceanography of the Peruvian margin during the last two millennia. Geochem. Geophys. Geosystems 9, Q05013. http://dx.doi.org/10.1029/2007GC001744.
Altabet, M.A., Francois, R., Murray, D.W., Prell, W.L., 1995. Climate-related variations in denitrification in the Arabian Sea from sediment $^{15}N/^{14}N$ ratios. Nature 373, 506–509. http://dx.doi.org/10.1038/373506a0.
Altabet, M.A., Higginson, M.J., Murray, D.W., 2002. The effect of millennial-scale changes in Arabian Sea denitrification on atmospheric CO_2. Nature 415 (6868), 159–162. http://dx.doi.org/10.1038/415159a.
Ashok, K., Behera, S.K., Rao, S.A., Weng, H., Yamagata, T., 2007. El Niño Modoki and its possible teleconnection. J. Geophys. Res. 112, C11007. http://dx.doi.org/10.1029/2006JC003798.
Avaria, S., Muñoz, P., 1987. Effects of the 1982–1983 El Niño on the marine phytoplankton off northern Chile. J. Geophys. Res. 92, 14369–14382. http://dx.doi.org/10.1029/JC092iC13p14369.
Barber, R.T., Chávez, F.P., 1986. Ocean variability in relation to living resources during the 1982–83 El Niño. Nature 319, 279–285. http://dx.doi.org/10.1038/319279a0.
Barber, R.T., Sanderson, M.P., Lindley, S.T., Chai, F., Newton, J., Trees, C.C., Foley, D.G., Chavez, F.P., 1996. Primary productivity and its regulation in the equatorial Pacific during and following the 1991–1992 El Niño. Deep-Sea Res. Part II Top. Stud. Oceanogr. 43 (4–6), 933–969. http://dx.doi.org/10.1016/0967-0645(96)00035-5.
Bjerknes, J., 1969. Atmospheric teleconnections from the equatorial Pacific. Mon. Weather Rev. 97, 163–172.
Brodie, I., Kemp, A.E.S., 1994. Variation in detrital fluxes and formation of laminae in late Quaternary sediments from the Peruvian coastal upwelling zone. Mar. Geol. 116, 385–398. http://dx.doi.org/10.1016/0025-3227(94)90053-1.
Chatfield, C., 1989. The Analysis of Time Series. Chapman & Hall, London.
Chavez, F.P., Barber, R.T., 1987. An estimate of new production in the equatorial Pacific. Deep Sea Res. 34, 1229–1243. http://dx.doi.org/10.1016/0198-0149(87)90073-2.
Chavez, F.P., 1995. A comparison of ship and satellite chlorophyll from California and Peru. J. Geophys. Res. 100, 24855–24862. http://dx.doi.org/10.1029/95JC02738.
Chavez, F.P., Buck, K.R., Service, S.K., Newton, J., Barber, R.T., 1996. Phytoplankton variability in the central and eastern tropical Pacific. Deep Sea Res. II 43, 835–870. http://dx.doi.org/10.1016/0967-0645(96)00028-8.
Chavez, F.P., Messié, M., 2009. A comparison of eastern boundary upwelling ecosystems. Prog. Oceanogr. 83, 80–96. http://dx.doi.org/10.1016/j.pocean.2009.07.032.
Cobb, K., Charles, C.D., Cheng, H., Edwards, R.L., 2003. El Niño Southern oscillation and tropical pacific climate during the last millennium. Nature 424, 271–276. http://dx.doi.org/10.1038/nature01779.
Conroy, J.L., Overpeck, J.T., Cole, J.E., Shanahan, T.M., Steinitz-Kannan, M., 2008. Holocene changes in eastern tropical Pacific climate inferred from a Galapagos lake sediment record. Quat. Sci. Rev. 27, 1166–1180. http://dx.doi.org/10.1016/j.quascirev.2008.02.015.
Conroy, J., Overpeck, J.T., Cole, J.E., 2010. El Niño/Southern oscillation and changes in the zonal gradient of tropical Pacific sea surface temperature over the last 1.2 ka. PAGES News 18 (1), 32–34.
Cowles, T., Barber, R., Guillen, O., 1977. Biological consequences of the 1975 El Niño. Science 195, 285–287. http://dx.doi.org/10.1126/science.195.4275.285.
Crosta, X., Koç, N., 2007. Diatoms: from micropaleontology to isotope geochemistry. Dev. Mar. Geol. 1, 327–369. http://dx.doi.org/10.1016/S1572-5480(07)01013-5.
Cruz, F.W., Burns, S.J., Karmann, I., Sharp, W.D., Vuille, M., Cardoso, A.O., Ferrari, J.A., Silva Dias, P.L., Viana, O., 2005. Insolation-driven changes in atmospheric circulation over the past 116,000 years in subtropical Brazil. Nature 434, 63–66. http://dx.doi.org/10.1038/nature03365.
Curry, R.G., McCartney, M.S., Joyce, T.M., 1998. Oceanic transport of subpolar climate signals to mid-depth subtropical waters. Nature 391, 575–577. http://dx.doi.org/10.1038/35356.
Davis, O.K., 1994. The correlation of summer precipitation in the southwestern USA with isotopic records of solar activity during the Medieval Warm Period. Clim. Change 26 (2–3), 271–287. http://dx.doi.org/10.1007/BF01092418.
Delworth, T., Mann, M.E., 2000. Observed and simulated multidecadal variability in the Northern Hemisphere. Clim. Dyn. 16, 661–676. http://dx.doi.org/10.1007/s003820000075.
De Pol-Holz, R., Ulloa, O., Lamy, F., Dezileau, L., Sabatier, P., Hebbeln, D., 2006. Late Quaternary variability of sedimentary nitrogen isotopes in the eastern South Pacific Ocean. Paleoceanography 22, L04704. http://dx.doi.org/10.1029/2005GL024477.
Dewitte, B., Vazquez-Cuervo, J., Goubanova, K., Illig, S., Takahashi, K., Cambon, G., Purca, S., Correa, D., Gutiérrez, D., Sifeddine, A., Ortlieb, L., 2012. Change in El Niño flavours over 1958–2008: implications for the long-term trend of the upwelling off Peru. Deep Sea Res. Part II Top. Stud. Oceanogr. 77, 143–156.
Diaz-Ochoa, J.A., Lange, C.B., Pantoja, S., De Lange, G.J., Gutiérrez, D., Muñoz, P., Salamanca, M., 2009. Fish scales in sediments from off Callao, central Peru. Deep Sea Res. II 56, 1124–1135. http://dx.doi.org/10.1016/j.dsr2.2008.09.015.
Diaz-Ochoa, J.A., Pantoja, S., De Lange, G.J., Sánchez, G.E., Acuña, V.R., Muñoz, P., Vargas, G., 2011. Oxygenation variability in Mejillones Bay, off northern Chile, during the last two centuries. Biogeosciences 8, 137–146. http://dx.doi.org/10.5194/bg-8-137-2011.
Dong, B., Sutton, R., Scaife, A.A., 2006. Multidecadal modulation of El Niño Southern oscillation (ENSO) variance by Atlantic ocean sea surface temperatures. Geophys. Res. Lett. 33, L08715. http://dx.doi.org/10.1029/2006GL025766.
Echevin, V., Aumont, O., Ledesma, J., Flores, G., 2008. The seasonal cycle of surface chlorophyll in the Peruvian upwelling system: a modeling study. Prog. Oceanogr. 79, 167–176. http://dx.doi.org/10.1016/j.pocean.2008.10.026.
Fiedler, P.C., Talley, L.D., 2006. Hydrography of the eastern tropical Pacific: a review. Prog. Oceanogr. 69, 143–180. http://dx.doi.org/10.1016/j.pocean.2006.03.008.
Fleury, S., 2015. Laminations sédimentaires et variabilité climatique et océanographique haute-fréquence sur la marge péruvienne. University of Bordeaux, France (PhD thesis).
Galbraith, E.D., Sigman, D.M., Robinson, R.S., Pedersen, T.F., 2008. Nitrogen in past marine environments. In: Capone, D.G., et al. (Eds.), Nitrogen in the Marine Environment, second ed. Academic, Burlington, Mass, pp. 1497–1535.
Ganeshram, R.S., Pedersen, T.F., Calvert, S.E., Murray, J.M., 1995. Large changes in oceanic inventories from glacial to interglacial periods. Nature 376, 755–758. http://dx.doi.org/10.1038/376755a0.
Garreaud, R.D., Vuille, M., Compagnucci, R., Marengo, J., 2009. Present-day South American climate. Palaeogeogr. Palaeoclimatol. Palaeoecol. 281, 180–195. http://dx.doi.org/10.1016/j.palaeo.2007.10.032.
Gilman, D.L., Fuglister, F.J., Mitchell Jr., J.M., 1963. On the power spectrum of "red noise". J. Atmos. Sci. 20, 182–184.
Graumlich, L.J., 1993. A 1000-year record of temperature and precipitation in the Sierra Nevada. Quat. Res. 39, 249–255. http://dx.doi.org/10.1006/qres.1993.1029.
Grove, J.M., 1988. The Little Ice Age (Methuen, London).
Gutiérrez, D., Enríquez, E., Purca, S., Quipúzcoa, L., Marquina, R., Flores, G., Graco, M., 2008. Oxygenation episodes on the continental shelf of central Peru: remote forcing and benthic ecosystem response. Prog. Oceanogr. 79, 177–189. http://dx.doi.org/10.1016/j.pocean.2008.10.025.
Gutiérrez, D., Sifeddine, A., Field, D.B., Ortlieb, L., Vargas, G., Chavez, F., Velazco, F., Ferreira, V., Tapia, P., Salvatecci, R., Boucher, H., Morales, M.C., Valdés, J., Reyss, J.-L., Campusano, A., Boussafir, M., Mandeng-Yogo, M., Garcia, M., Baumgartner, T., 2009. Rapid reorganization of ocean biogeochemistry off Peru towards the end of the Little Ice Age. Biogeosciences 6, 835–848. http://dx.doi.org/10.5194/bg-6-835-2009.
Hasle, G.R., Syvertsen, E., 1996. Marine diatoms. In: Thomas, C. (Ed.), Identifying Marine Diatoms and Dinoflagellates. Academic Press, San Diego, p. 385.
Haug, G.H., Hughen, K.A., Sigman, D.M., Peterson, L.C., Röhl, U., 2001. Southward migration of the Intertropical Convergence Zone through the Holocene. Science 293, 1304–1308. http://dx.doi.org/10.1126/science.1059725.
Hendy, I.L., Pedersen, T.F., 2006. Oxygen minimum zone expansion in the eastern tropical North Pacific during deglaciation. Geophys. Res. Lett. 33 (20) http://dx.doi.org/10.1029/2006GL025975.
Hodell, D.A., Brenner, M., Curtis, J.H., Medina-Gonzalez, R., Ildefonso-Chan Can, E., Albornaz-Pat, A., Guilderson, T.P., 2005. Climate change on the Yucatan Peninsula during the Little Ice Age. Quat. Res. 63, 109–121. http://dx.doi.org/10.1016/j.yqres.2004.11.004.
Horel, J., Cornejo-Garrido, A., 1986. Convection along the coast of Northern Peru during 1983: spatial and temporal variation of clouds and rainfall. Mon. Weather Rev. 114, 2091–2105 doi: 10.1175/1520-0493(1986)114<2091:CATCON>2.0CO;2.
Huffman, G.J., Adler, R.F., Bolvin, D.T., Gu, G., 2009. Improving the global precipitation record: GPCP version 2.1. Geophys. Res. Lett. 36 (17) http://dx.doi.org/10.1029/2009GL040000.
Jenkins, G.M., Watts, D.G., 1968. Spectral Analysis and its Applications. Holden-Day, San Francisco.
Jones, P.D., Briffa, K.R., Barnett, T.P., Tett, S.F.B., 1998. High resolution palaeoclimatic records for the last millennium: integration, interpretation and comparison with General Circulation Model control run temperatures. Holocene 8, 455–471.
Julian, P.R., Chervin, R.M., 1978. A study of the Southern oscillation and Walker circulation phenomenon. Mon. Weather Rev. 106, 1433–1451 doi: 10.1175/1520-0493(1978)106<1433:ASOTSO>2.0.CO;2.
Jungclaus, J.H., Haak, H., Latif, M., Mikolajewicz, U., 2005. Arctic-North Atlantic interactions and multi-decadal variability of the Meridional overturning Circulation. J. Clim. 18, 4013–4031. http://dx.doi.org/10.1175/JCLI3462.1.
Kao, H.-Y., Yu, J.-Y., 2009. Contrasting Eastern-Pacific and Central-Pacific types of ENSO. J. Clim. 22, 615–632. http://dx.doi.org/10.1175/2008JCLI2309.1.
Kessler, W.S., McPhaden, M.J., 1995. Oceanic equatorial waves and the 1991–1993 El Niño. J. Clim. 8, 1757–1774 doi: 10.1175/1520-0442(1995)008<1757:OEWATE>2.0CO;2.
Knight, J.R., Allan, R.J., Folland, C.K., Vellinga, M., Mann, M.E., 2005. A signature of persistent thermohaline circulation cycles in observed climate. Geophys. Res. Lett. 32, L20708. http://dx.doi.org/10.1029/2005GL024233.
Knight, J.R., Folland, C.K., Scaife, A.A., 2006. Climate impacts of the Atlantic multidecadal oscillation. Geophys. Res. Lett. 33, L17706. http://dx.doi.org/10.1029/

2006GL026242.
Krissek, L.A., Scheidegger, K.F., Kulm, L.D., 1980. Surface sediments of the Peru-Chile continental margin and the Nazca plate. Geol. Soc. Am. Bull. 91 (6), 321–331. http://dx.doi.org/10.1130/0016-7606(1980)91<321.
Lamb, H.H., 1985. Climatic History and the Future. Princeton University Press, Princeton, NJ, p. 835.
Lau, K.-M., Weng, H.-Y., 1995. Climate signal detection using wavelet transform: how to make a time series sing. Bull. Am. Meteorol. Soc. 76, 2391–2402.
Leduc, G., Vidal, L., Tachikawa, K., Bard, E., 2009. ITCZ rather than ENSO signature for abrupt climate changes across the tropical Pacific? Quat. Res. 72, 123–131. http://dx.doi.org/10.1016/j.yqres.2009.03.006.
Levitus, S., Boyer, T.P., 1994. World Ocean Atlas 1994. In: Oxygen (No. PB-95-270096/XAB; NOAA-ATLAS-2), vol. 2. National Environmental Satellite, Data, and Information Service, Washington, DC (United States).
Li, J., Xie, S.-P., Cook, E.R., Huang, G., D'Arrigo, R., Liu, F., Ma, J., Zheng, X.-T., 2011. Interdecadal modulation of El Niño amplitude during the last millennium. Nat. Clim. Change 1 (2), 114–118. http://dx.doi.org/10.1038/NCLIMATE1086.
Li, J., Xie, S.-P., Cook, E.R., Morales, M.S., Christie, D.A., Johnson, N.C., Chen, F., D'Arrigo, R., Fowler, A.M., Gou, X., Fang, K., 2013. El Niño modulations over the past seven centuries. Nat. Clim. Change 3, 822–826. http://dx.doi.org/10.1038/NCLIMATE1936.
Lund, D.C., Lynch-Stieglitz, J., Curry, W.B., 2006. Gulf Stream density structure and transport during the past millennium. Nature 444, 601–604. http://dx.doi.org/10.1038/nature05277.
Mann, M.E., Bradley, R.S., Hughes, M.K., 1999. Northern Hemisphere temperatures during the past millennium: inferences, uncertainties and limitations. Geophys. Res. Lett. 26, 759–762. http://dx.doi.org/10.1029/1999GL900070.
Mann, M.E., Cane, M.A., Zebiak, S.E., Clement, A., 2005. Volcanic and solar forcing of the tropical Pacific over the past 1000 years. J. Clim. 18, 417–456, 1175/JCLI-3276-1.
McManus, J.F., François, R., Gherardi, J.-M., Keigwin, L.D., Brown-Leger, S., 2004. Collapse and rapid resumption of Atlantic meridional circulation linked to deglacial climate changes. Nature 428, 834–837. http://dx.doi.org/10.1038/nature02494.
Messié, M., Ledesma, J., Kolber, D.D., Michisaki, R.P., Foley, D.G., Chavez, F.P., 2009. Potential new production estimates in four eastern boundary upwelling ecosystems. Prog. Oceanogr. 83, 151–158. http://dx.doi.org/10.1016/j.pocean.2009.07.018.
Meyers, P.A., 1997. Organic geochemical proxies of paleoceanographic, paleolimnologic and paleoclimatic processes. Org. Geochem. 27, 213–250. http://dx.doi.org/10.1016/S0146-6380(97)00049-1.
Migeon, S., Weber, O., Faugeres, J.-C., Saint-Paul, J., 1999. SCOPIX: a new X-ray imaging system for core analysis. Geo-Marine Lett. 18, 251–255. http://dx.doi.org/10.1007/s003670050076.
Mollier-Vogel, E., 2012. Peruvian Oxygen Minimum Zone Dynamics during the Last 18 000 Years. University of Kiel, Germany (PhD thesis).
Mollier-Vogel, E., Ryabenko, E., Martinez, P., Wallace, D., Altabet, M.A., Schneider, R., 2012. Nitrogen isotope gradients off Peru and Ecuador related to upwelling, productivity, nutrient uptake and oxygen deficiency. Deep Sea Res. Part I Oceanogr. Res. Pap. 70, 14–25. http://dx.doi.org/10.1016/j.dsr.2012.06.003.
Mollier-Vogel, E., Leduc, G., Böschen, T., Martinez, P., Schneider, R., 2013. Rainfall response to orbital and millenial forcing in northern Peru over the last 18 ka. Quat. Sci. Rev. 76, 29–38. http://dx.doi.org/10.1016/j.quascirev.2013.06.021.
Montecino, V., Lange, C.B., 2009. The Humboldt Current System: ecosystem components and processes, fisheries and sediment studies. Prog. Oceanogr. 83, 65–79. http://dx.doi.org/10.1016/j.pocean.2009.07.041.
Morales, M. del C., Field, D., Mayor Pastor, S., Gutiérrez, D., Sifeddine, A., Ortlieb, L., Ferreira, V., Salvatecci, R., Velazco, F., 2006. Variaciones de foraminíferos de los últimos 460 años en sedimentos laminados de la plataforma continental peruana. Bol. Soc. Geol. Perú 101, 5–18.
Moreno, A., Pérez, A., Frigola, J., Nieto-Moreno, V., Rodrigo-Gámiz, M., Martrat, B., González-Sampériz, P., Morellón, M., Martín-Puertas, C., Corella, J.P., Belmonte, A., Sancho, C., Cacho, I., Herrera, G., Canals, M., Grimalt, J.O., Jimenéz-Espejo, F., Martínez-Ruiz, F., Vegas-Villarrúbia, T., Valero-Garcés, B.L., 2012. The Medieval Climate Anomaly in the Iberian Peninsula reconstructed from marine and lake records. Quat. Sci. Rev. 43, 16–32. http://dx.doi.org/10.1016/j.quascirev.2012.04.007.
Moreno, J.L., Licea, S., Santoyo, H., 1996. Diatomeas del golfo de California. Universidad autónoma de Baja California Sur, p. 274.
Moy, M.C., Seltzer, G.O., Rodbell, D.T., Anderson, D.M., 2002. Variability of El Niño/Southern oscillation activity at millenial timescales during the Holocene epoch. Nature 420, 162–165. http://dx.doi.org/10.1038/nature01194.
Olsen, J., Anderson, J.N., Knudsen, M.F., 2012. Variability of the North Atlantic oscillation over the past 5200 years. Nat. Geosci. 5, 808–812. http://dx.doi.org/10.1038/ngeo1589.
Ortlieb, L., Macharé, J., 1993. Former El Niño events: records from western South America. Glob. Planet. Change 7 (1), 181–202. http://dx.doi.org/10.1016/0921-8181(93)90049-T.
Ortlieb, L., Vargas, G., Saliège, J.-F., 2011. Marine radiocarbon reservoir effect along the northern Chile-southern Peru coast (14–24°S) throughout the Holocene. Quat. Res. 75, 91–103. http://dx.doi.org/10.1016/j.yqres.2010.07.018.
Paillard, D., Labeyrie, L., Yiou, P., 1996. Macintosh program performs time-series analysis. Eos, Trans. Am. Geophys. Union 77, 379. http://dx.doi.org/10.1029/96EO00259.
Pennington, J.T., Mahoney, K.L., Kuwahara, V.S., Kolber, D.D., Calienes, R., Chavez, F.P., 2006. Primary production in the eastern tropical Pacific: a review. Prog. Oceanogr. 69, 285–317. http://dx.doi.org/10.1016/j.pocean.2006.03.012.
Philander, S.G., 1990. El Niño, La Niña and the Southern Oscillation. Academic press, San Diego, p. 289.
Pichevin, L., Bard, E., Martinez, P., Billy, I., 2007. Evidence of ventilation changes in the Arabian Sea during the late Quaternary: implication for denitrification and nitrous oxide emission. Glob. Biogeochem. Cycles 21 (4), GB4008. http://dx.doi.org/10.1029/2006GB002852.
Rathburn, A.E., Pichon, J.-J., Ayress, M.A., De Deckker, P., 1997. Microfossil and stable-isotope evidence for changes in the late Holocene paleoproductivity and paleoceanographic conditions in the Prydz Bay region of Antarctica. Palaeogeogr. Palaeoclimatol. Palaeoecol. 131, 485–510. http://dx.doi.org/10.1016/S0031-0182(97)00017-5.
Reimer, P.J., Baillie, M.G.L., Bard, E., Bayliss, A., Beck, J.W., Blackwell, P.G., Ramsey, C.B., Buck, C.E., Burr, G.S., Edwards, R.L., Friedrich, M., Grootes, P.M., Guilderson, T.P., Hajdas, I., Heaton, T.J., Hogg, A.G., Hughen, K.A., Kaiser, K.F., Kromer, B., McCormac, F.G., Manning, S.W., Reimer, R.W., Richards, D.A., Southon, J.R., Talamo, S., Turney, C.S.M., van der Plicht, J., Weyhenmeyer, C.E., 2009. IntCal09 and Marine09 radiocarbon age calibration curves, 0-50,000 years cal BP. Radiocarbon 51, 1111–1150.
Rein, B., Lückge, A., Sirocko, F., 2004. A major Holocene ENSO anomaly during the Medieval Warm period. Geophys. Res. Lett. 31, L17211. http://dx.doi.org/10.1029/2004GL020161.
Rein, B., Lückge, A., Reinhardt, L., Sirocko, F., Wolf, A., Dullo, W.-C., 2005. El Niño variability off Peru during the last 20,000 years. Paleoceanography 20, PA4003. http://dx.doi.org/10.1029/2004PA001099.
Reuter, J., Stott, L., Khider, D., Sinha, A., Cheng, H., Edwards, R.L., 2009. A new perspective on the hydroclimate variability in northern South America during the Little Ice Age. Geophys. Res. Lett. 36, L21706. http://dx.doi.org/10.1029/2009GL041051.
Richter, T.O., van der Gaast, S., Koster, B., Vaars, A., Gieles, R., de Stigter, H.C., de Haas, H., Van Weering, T.C.E., 2006. The Avaatech XRF Core Scanner: technical description and applications to NE Atlantic sediments. In: Rothwell, R.G. (Ed.), New Techniques in Sediment Core Analysis, Geological Society of London, Special Publications, pp. 39–50.
Robbins, J.A., Edgington, D.N., 1975. Determination of recent sedimentation rates in Lake Michigan using Pb-210 and Cs-137. Geochim. Cosmochim. Acta 39, 285–304. http://dx.doi.org/10.1016/0016-7037(75)90198-2.
Robinson, R.S., Mix, A., Martinez, P., 2007. Southern ocean control on the extent of denitrification in the southeast Pacific over the last 70ka. Quat. Sci. Rev. 26 (1), 201–212. http://dx.doi.org/10.1016/j.quascirev.2006.08.005.
Sachs, J.P., Sachse, D., Smittenberg, R.K., Zhang, Z., Battisti, D.S., Golubic, S., 2009. Southward movement of the Pacific intertropical convergence zone AD 1400–1850. Nat. Geosci. 2, 519–525. http://dx.doi.org/10.1038/NGEO554.
Saenger, C., Chang, P., Ji, L., Oppo, D.W., Cohen, A.L., 2009. Tropical Atlantic climate response to low-latitude and extratropical sea-surface temperature: a Little Ice Age perspective. Geophys. Res. Lett. 36, L11703. http://dx.doi.org/10.1029/2009GL038677.
Salvatteci, R., Gutiérrez, D., Field, D., Sifeddine, A., Ortlieb, L., Bouloubassi, I., Boussafir, M., Boucher, H., Cetin, F., 2014. The response of the Peruvian Upwelling Ecosystem to centennial-scale global change during the last two millennia. Clim. Past 10 (2), 715–731. http://dx.doi.org/10.5194/cp-10-715-2014.
Sar, E., Sunesen, I., Castaños, C., 2001. Marine diatoms from Buenos Aires coastal waters (República Argentina). I. Thalassiosiraceae. Nova Hedwig. 73, 199–228.
Sar, E., Sunesen, I., Lavigne, A.S., 2002. The diatom genus Thalassiosira: species from the northern San Matías Gulf (Río Negro, Argentina). Nova Hedwig. 74, 373–386.
Sarno, D., Kooistra, W.H.C.F., Medlin, L.K., Percopo, I., Zingone, A., 2005. Diversity in the genus Skeletonema (Bacillariophyceae). II. An assessment of the taxonomy of *S. costatum*-like species with the description of four new species. J. Phycol. 41, 151–176.
Scheidegger, K.F., Krissek, L.A., 1982. Dispersal and deposition of eolian and fluvial sediments off Peru and northern Chile. Geol. Soc. Am. Bull. 93 (2), 150–162. http://dx.doi.org/10.1130/0016-7606(1982)93<150.
Schmidt, S., Harlay, J., Borges, A.V., Groom, S., Delille, B., Roevros, N., Christodoulou, S., Chou, L., 2013. J. Mar. Syst. 109–110, S 182–190. http://dx.doi.org/10.1016/j.jmarsys.2011.12.005.
Scholz, F., McManus, J., Mix, A.C., Hensen, C., Schneider, R.R., 2014. The impact of ocean deoxygenation on iron release from continental margin sediments. Nat. Geosci. 7, 433–437. http://dx.doi.org/10.1038/ngeo2162.
Sicre, M.-A., Jacob, J., Ezat, U., Rousse, S., Kissel, C., Yiou, P., Eiriksson, J., Knudsen, K.L., Jansen, E., Turon, J.-L., 2008. Decadal variability of sea surface temperatures off North Iceland over the last 2000 years. Earth Planet. Sci. Lett. 268, 137–142. http://dx.doi.org/10.1016/j.epsl.2008.01.011.
Sifeddine, A., Gutiérrez, D., Ortlieb, L., Boucher, H., Velazco, F., Field, D.B., Vargas, G., Boussafir, M., Salvatecci, R., Ferreira, V., Garcia, M., Valdés, J., Caquineau, S., Mandeng-Yogo, M., Solis, J., Soler, P., Baumgartner, T., 2008. Laminated sediments from the central Peruvian continental slope: a 500-year record of upwelling system productivity, terrestrial runoff and redox conditions. Prog. Oceanogr. 79, 190–197. http://dx.doi.org/10.1016/j.pocean.2008.10.024.
Strub, P.T., Mesias, J.M., Montecino, V., Rutllant, J., Salinas, S., 1998. Coastal ocean circulation off Western South America (coastal segment). In: Robinson, A., Brink, K. (Eds.), The Global Coastal Ocean. Wiley, New York.
Stuiver, M., Reimer, P.J., 1993. Extended ^{14}C database and revised CALIB radiocarbon calibration program. Radiocarbon 35, 215–230.

Stuiver, M., Grootes, P.M., Braziunas, T.F., 1995. The GISP2 N18O climate record of the past 16,500 years and the role of the sun, ocean and volcanoes. Quat. Res. 44, 341–354. http://dx.doi.org/10.1006/qres.1995.1079.

Sundström, B.G., 1986. The Marine Diatom Genus Rhizosolenia. A New Approach to the Taxonomy. University of Lund, Sweden (PhD thesis).

Sunesen, I., Hernández-Becerril, D.U., Sar, E.A., 2008. Marine diatoms from Buenos Aires coastal waters (Argentina). V. Species of the genus Chaetoceros. Rev. Biol. Mar. Oceanogr. 43, 303–326.

Swingedouw, D., Terray, L., Cassou, C., Voldoire, A., Salas-Mélia, D., Servonnat, J., 2011. Natural forcing of climate during the last millennium: fingerprint of solar variability. Low frequency solar forcing and NAO. Clim. Dyn. 36, 1349–1364. http://dx.doi.org/10.1007/s00382-010-0803-5.

Thunell, R.C., Kepple, A.B., 2004. Glacial-Holocene d^{15}N record from the Gulf of Tehuantepec, Mexico: Implications for denitrification in the eastern equatorial Pacific and changes in atmospheric N_2O. Glob. Biogeochem. Cycles 18, GB1001. http://dx.doi.org/10.1029/2002GB002028.

Timmermann, A., Okumura, Y., An, S.-I., Clement, A., Dong, B., Guilyardi, E., Hu, A., Jungclaus, J.H., Renold, M., Stocker, T.F., Stouffer, R.J., Sutton, R., Xie, S.-P., Yin, J., 2007. The influence of a weakening of the Atlantic meridional overturning circulation on ENSO. J. Clim. 20, 4899–4919. http://dx.doi.org/10.1175/JCLI4283.1.

Toggweiler, J., Dixon, K., Broecker, W., 1991. The Peru upwelling and the ventilation of the South Pacific thermocline. J. Geophys. Res. 96, 20467–20497. http://dx.doi.org/10.1029/91JC02063.

Torrence, C., Compo, G.P., 1998. A practical guide to wavelet analysis. Bull. Am. Meteorol. Soc. 79, 61–78.

Trouet, V., Esper, J., Graham, N.E., Baker, A., Scourse, J.D., Frank, D.C., 2009. Persistent positive North Atlantic oscillation mode dominated the medieval climate anomaly. Science 324, 5923. http://dx.doi.org/10.1126/science.1166349.

Vargas, G., Ortlieb, L., Pichon, J.-J., Bertaux, J., Pujos, M., 2004. Sedimentary facies and high-resolution primary production inferences from laminated diatomaceous sediments off northern Chile (23°S). Mar. Geol. 211, 79–99. http://dx.doi.org/10.1016/j.margeo.2004.05.032.

Vargas, G., Pantoja, S., Rutland, J.A., Lange, C.B., Ortlieb, L., 2007. Enhancement of coastal upwelling and interdecadal ENSO-like variability in the Peru-Chile current since late 19th century. Geophys. Res. Lett. 34, L13607. http://dx.doi.org/10.1029/2006GL028812.

Wang, X., Auler, A.S., Edwards, R.L., Cheng, H., Ito, E., Wang, Y., Kong, X., Solheid, M., 2007. Millenial-scale precipitation changes in southern Brazil over the past 90,000 years. Geophys. Res. Lett. 34, L23701. http://dx.doi.org/10.1029/2007GL031149.

Wassenburg, J.A., Immenhauser, A., Richter, D.K., Niedermayr, A., Riechelmann, S., Fietzke, J., Scholz, D., Jochum, K.P., Fohlmeister, J., Schröder-Ritzau, A., Sabaoui, A., Riechelmann, D.F.C., Schneider, L., Esper, J., 2013. Earth Planet. Sci. Lett. 375, 291–302. http://dx.doi.org/10.1016/j.epsl.2013.05.048.

Wells, L.E., 1990. Holocene history of the El Niño phenomenon as recorded in flood sediments of northern coastal Peru. Geology 18, 1134–1137 doi: 10.1130/0091-7613(1990)018<1134:HHOTEN>2.3.CO;2.

Weng, H., Ashok, K., Behera, S.K., Rao, S.A., Yamagata, T., 2007. Impacts of recent El Niño Modoki on dry/wet conditions in the Pacific rim during boreal summer. Clim. Dyn. 29, 113–129. http://dx.doi.org/10.1007/s00382-007-0234-0.

Wolf, A., 2002. Zeitlische Variationen im peruanischen Küstenauftrieb seit dem letzten glazialen Maximum-Steuerung durch globale Klimadynamik. University of Kiel, Germany (PhD thesis).

Wolff, C., Haug, G.H., Timmermann, A., Sinninghe Damsté, J.S., Brauer, A., Sigman, D.M., Cane, M.A., Verschuren, D., 2011. Reduced interannual rainfall variability in East Africa during the Little Ice Age. Science 333, 743–747. http://dx.doi.org/10.1126/science.1203724.

Wu, L., He, F., Liu, Z., 2005. Coupled ocean-atmosphere response to north tropical Atlantic SST: tropical Atlantic dipole and ENSO. Geophys. Res. Lett. 32, L21712. http://dx.doi.org/10.1029/2005GL024222.

Wyrtki, K., 1981. An estimate of equatorial upwelling in the Pacific. J. Phys. Oceanogr. 11, 1205–1214. http://dx.doi.org/10.1175/1520-0485(1981)011.

Xie, S.P., Miyama, T., Wang, Y., Xu, H., de Szoeke, S.P., Small, R.J.O., Richards, K.J., Mochizuki, T., Awaji, T., 2007. A regional ocean-atmosphere model for eastern Pacific climate: toward reducing tropical biases. J. Clim. 20, 1504–1522. http://dx.doi.org/10.1175/JCLI4080.1.

Yan, H., Sun, L., Wang, Y., Huang, W., Qiu, S., Yang, C., 2011. A record of the Southern oscillation Index for the past 2,000 years from precipitation proxies. Nat. Geosci. 4 (9), 611–614. http://dx.doi.org/10.1038/NGEO1231.

Zhang, P., Cheng, H., Edwards, R.L., Chen, F., Wang, Y., Yang, X., Liu, J., Tan, M., Wang, X., Liu, J., An, C., Dai, Z., Zhou, J., Zhang, D., Jia, J., Jin, L., Johnson, K.R., 2008. A test of climate, sun and culture relationships from an 1810-year Chinese cave record. Science 322, 940–942. http://dx.doi.org/10.1126/science.1163965.